Key Engineering Materials
ISSN: 1662-9795, Vol. 926, pp 875-882
doi:10.4028/p-14s93w

Submitted: 2021-12-13
Revised: 2022-02-08
Accepted: 2022-02-08
Online: 2022-07-22

Analysis of Thickness Distributions Calculated from Surface Strains Obtained through Digital Image Correlation for Incremental Sheet Forming

M. Vanhulst[1,a*], H. Vanhove[1,b], Y. Carette[1,c], S. Waumans[1,d] and J.R. Duflou[1,e]

[1]Department of Mechanical Engineering, Katholieke Universiteit Leuven / Flanders Make, Celestijnenlaan 300B, B-3001 Leuven, Belgium

[a]marthe.vanhulst@kuleuven.be; [b]hans.vanhove@kuleuven.be; [c]yannick.carette@kuleuven.be; [d]stijn.waumans@kuleuven.be; [e]joost.duflou@kuleuven.be

Keywords: Incremental Sheet Forming, Process Control, Digital Image Correlation, Strain Fields, Thickness Distributions

Abstract. This paper discusses the thickness distributions calculated from surface strain measurements using stereo Digital Image Correlations (DIC) for parts produced with Single Point Incremental Forming (SPIF). The research is carried out on six benchmark cones and pyramids with each convex, straight and concave walls. The accuracy of the thickness calculations, under the assumption of material incompressibility and using the formula for the Green-Lagrange strains, is compared to the thickness distributions measured with a fringe projection scanner. The thickness estimations based on the measured strains proved to be representative for the measured thickness distributions with a mean error of 0.0182 mm, which corresponds to a relative error of 1.47 % of the mean measured thickness. However, errors of up to 0.1688 mm were found in areas of high wall angles and curvatures, corresponding to a relative maximal error of 13.69 % of the mean measured thickness. Hence, the DIC measurements are well suited for characterizing the thickness. Using the thicknesses calculated from the DIC measurements to find the minimal thickness as an indicator of part failure, is possible with relative errors that have an average overestimation of 2.87% of the minimal measured thickness.

Introduction

As a highly flexible sheet metal forming process, one of the principal features of Single Point Incremental Forming (SPIF) is the elimination of costly dies [1]. This makes the process especially suitable in case of small lot sizes and for customised parts. However, two challenges still prevent application in industrial settings. The first challenge is the limited geometric accuracy [1], which can be increased by applying compensation strategies based on the deviation between the desired geometry and the measured or predicted process outcome. The second challenge is the restricted process window [2]. Here, multistage strategies can improve the application range. In contrast to a single stage approach, the thickness distributions do not follow the approximation of the sine law anymore for multistage SPIF, but instead depend on the shapes of the intermediate steps [2]. These shapes highly influence the material trajectory and hence the thickness distributions. Therefore, with the thickness distributions as an indicator for part failure, intermediate shapes should be chosen in such a way that the material is steered to obtain a more uniform thickness distribution. The creation of optimal intermediate shapes requires specific knowledge and insight in the multistage process, which can be acquired using Digital Image Correlation (DIC) [3].

DIC techniques track material elements during deformations by correlating a speckle pattern in two or three dimensions, thereby enabling the calculation of the surface strains. A part with a random, non-repetitive speckle pattern is measured with two cameras for stereo DIC, taking subsequent images that represent the current state of the object. The images of both cameras are taken simultaneously in each time step, with the initial images as a reference state. The DIC software then correlates each unique subset in the region of interest, resulting in a three-dimensional displacement

field. Additional computations can be performed by the software on the obtained displacements to calculate the local surface strains and stresses for each time step.

This knowledge of the material trajectory and accompanying strains provides insight in the process and is particularly useful in multistage approaches for creating optimal intermediate shapes. Combining DIC experiments with separate thickness measurements is time-consuming and can be avoided if the thickness estimations calculated from the surface strains in DIC are representative for the measured thickness distributions.

DIC has been applied in literature to track the material trajectory and to characterise failure for the SPIF process [2, 4–9]. Thickness calculations based on DIC measurements have been validated for processes such as thermoforming and SPIF [10]–[12] but a more thorough investigation will be discussed here. This paper will focus on comparing the calculated thickness distributions from the surface strains (measured with DIC software) with the real thickness distributions after production with SPIF (measured with a fringe projection scanner).

Strain Definitions and Wall Thickness

The surface strains measured with stereo DIC can be used to calculate the thickness distributions based on the law of conservation of volume, assuming material incompressibility:

$$xyz = (x + dx)(y + dy)(z + dz). \tag{1}$$

The Green-Lagrange strain used in the strain calculation is described by the following formula:

$$\epsilon = \frac{1}{2}(\lambda^2 - 1) \tag{2}$$

with ϵ the strain and λ the ratio of the final length over the initial length.

Van Mieghem et al. [11] used these strains to derive the following formula for the resulting sheet thickness after deformation:

$$t_f = t_i \left(\frac{1}{\sqrt{(1+2\epsilon_1)(1+2\epsilon_2)}} \right). \tag{3}$$

With t_i the initial sheet thickness and ϵ_1 and ϵ_2 respectively the maximum and minimum principal strains after deformation.

Experiments

The experiments are conducted on 225x225 mm sheets of Aluminium alloy 5754 ($AlMg_3$) with a thickness of 1.5 mm on a KUKA KR500MT robotic arm. Two categories of shapes are produced: cones and pyramids. Both categories contain three main curvature types: concave, straight and convex (see Figure 1).

This gives a total of six experimental benchmark shapes that represent different workpiece geometries. The results contain areas of low, high and intermediate curvatures. The benchmark parts are designed in such a way that a wall angle of 60 degrees is not exceeded. This maximum angle is chosen well under the critical wall angle of 71 degrees for $AlMg_3$ sheets of 1.5 mm [13] in order to avoid failure.

The sheet is clamped along its circumference on a backing plate with a 184x184 mm squared orifice for the pyramids and a circular hole of 197 mm diameter for the cones. The tool of diameter 10 mm describes a spiralling toolpath with a scallop width of 0.6 mm at a feedrate of 4000mm/min. The sheet is lubricated with Nuto 46 oil prior to forming.

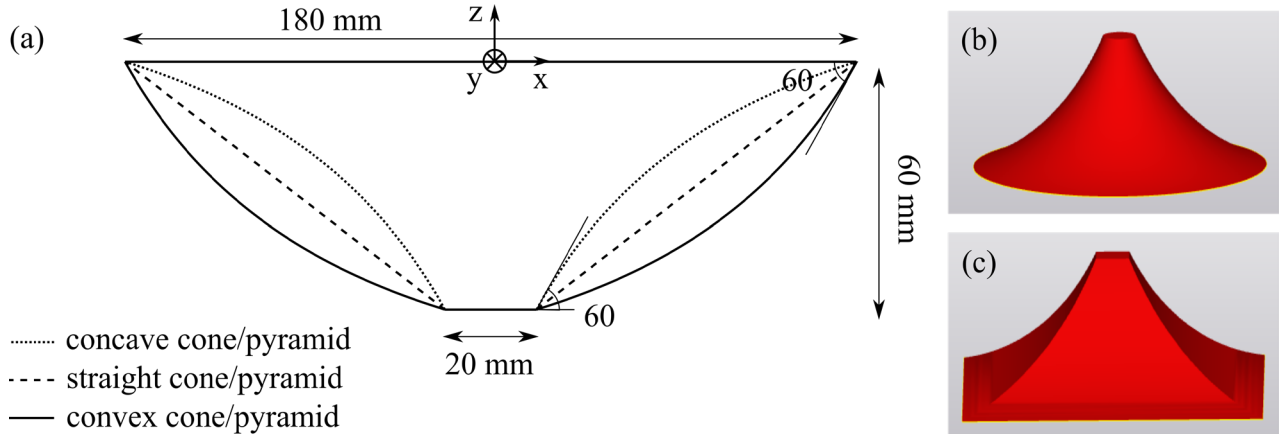

Figure 1: Sketch of the convex, straight and concave cones and pyramids (a) and CAD-models of the concave benchmark cone (b) and pyramid (c).

DIC setup. Two Mako G-507B Allied Vision cameras are equipped with Edmund Optics lenses with a focal length of 35 mm and are mounted at a distance of 620 mm from the sheet. Diffuse lighting conditions are created by using two DC-LED lights that aim towards a concave white shield to diffuse the light (Figure 2). The field of view is the bottom half of the part, since all shapes are symmetrical and to make sure the cameras can view all deformed speckles in the field of view at all times during and after production. The angle between the cameras in the horizontal direction is 23.56 degrees.

The 225 x 225 mm $AlMg_3$ sheets of 1.5 mm thick are screen printed black on white with a dotted random and high contrast speckle pattern. The average speckle size is 6.8 pixels with a black/white ratio of 87% (a ratio of 100% means that black and white are both 50% and the contrast is optimal). Images are taken each time the tool passes by the top of the part (at the negative y-axis at x=0 in Figure 2), which is outside the field of view to reduce the influence of the elastic local deformations in the vicinity of the tool tip on the correlation. Reference images are taken before forming and images of the final shape are captured after finishing the toolpath.

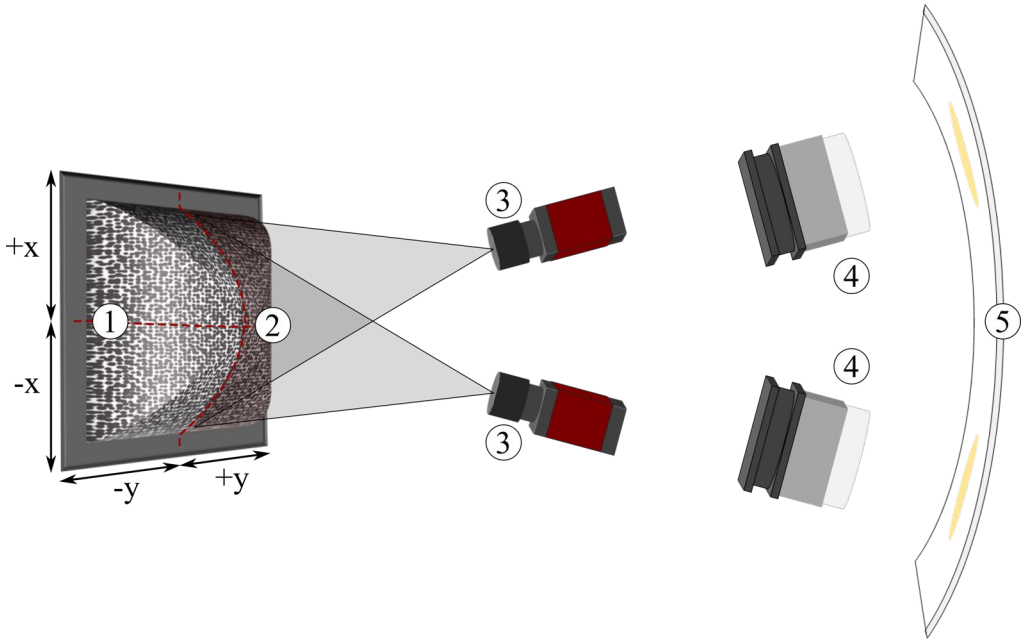

Figure 2: DIC setup with (1) the clamped part, (2) the field of view, (3) the cameras, (4) the spotlights and (5) a concave shield to diffuse the light.

The correlation calculations are performed with the MatchID Stereo software[1]. The correlation parameters are shown in Table 1. The stereo correlation in MatchID is determined with incremental correlation: the reference image is updated with the current one at each time step. After correlation,

[1] https://www.matchid.eu/

the data is transformed to the coordinate system of the part by indicating the x- and y-axes on the initial flat sheet. The strains are calculated on the transformed data with the Green-Lagrange formula (Formula 2) with 9 degrees of freedom (DoF) and a strain window of 15 pixels.

Table 1: Correlation parameters.

Correlation software	MatchID
Subset size [pixels]	39x39
Step size [pixels]	10
Correlation algorithm	Zero-Normalised Sum of Squared Differences (ZNSSD)
Interpolation	Bicubic Spline Interpolation
Shape function	Quadratic
Stereo transformation	Quadratic
Strain window [pixels]	15
Virtual Strain Gauge (VSG) [pixels]	179

GOM setup. The thickness distributions are measured with a GOM ATOS Compact Scan fringe projection scanner. The produced parts were coated with a light layer of white developer spray to avoid diffuse reflection of the projector on the metal.

Results and Discussion

The Green-Lagrange strains measured with the MatchID stereo DIC setup for the concave cone and pyramid are shown in Figure 3. Only a small part of the shape is considered as the region of interest (ROI), since the parts are symmetrical and to make sure every subset in the region of interest is visible by both cameras at all time steps.

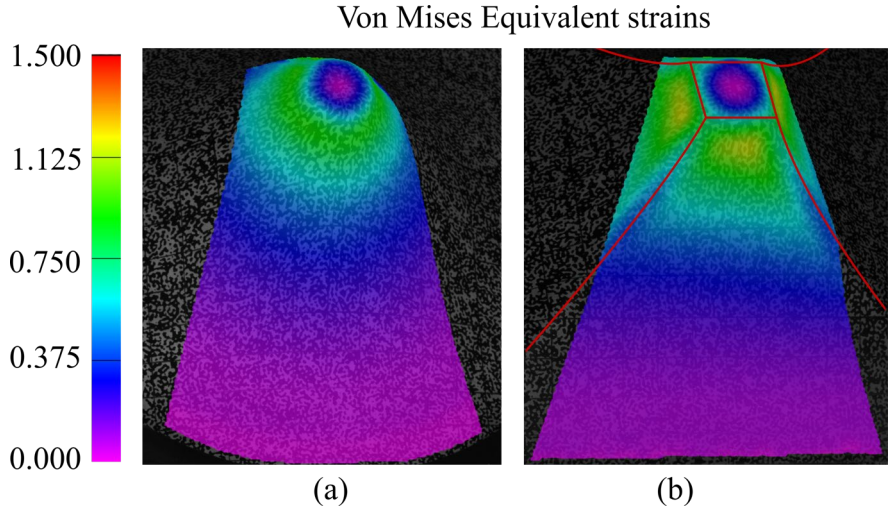

Figure 3: Von Mises Equivalent strains in MatchID for the region of interest of the concave cone (a) and the concave pyramid (b), calculated with the Green-Lagrange formula, 9 DoFs and a strain window of 15 pixels.

Figure 4 displays the differences between the thickness distributions measured with the GOM fringe projection scanner and the estimated distributions calculated from the DIC surface strains. The figure shows that the calculated thickness distributions follow the measured distributions well. The y-axes of the figures of the pyramids (Figure 4(b), (d) and (f)) are mirrored for visualisation.

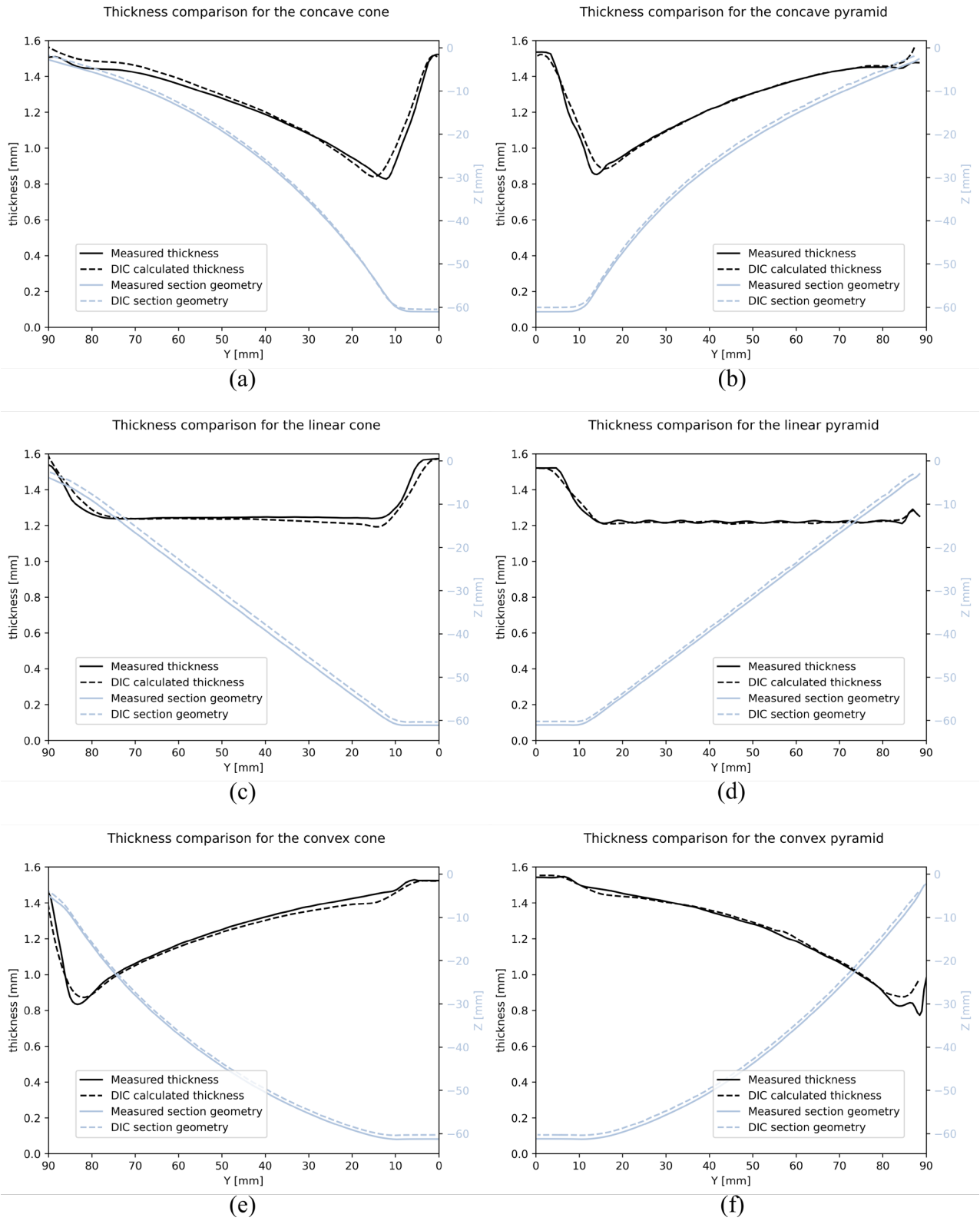

Figure 4: Comparison of the thickness distributions measured with the fringe projection scanner and the thickness distributions calculated from the DIC surface strain measurements at X=0 for concave (a), straight (c) and convex (e) cones and pyramids (respectively (b), (d) and (f)).

Tables 2-4 show the errors between the thickness and section curves for constant y-values, as well as the overall mean and minimal values of the measured and calculated thicknesses. The maximal and mean errors are calculated as the absolute value of the difference between the measured and calculated values for the thicknesses and z- coordinates at fixed y-values:

$$e_{t,i} = \left|t_{i,meas} - t_{i,calc}\right| \text{ and } e_{z,i} = \left|z_{i,meas} - z_{i,calc}\right| \quad (4)$$

for $i \in [1, N]$, N the number of y-values, $t_{i,meas}$ and $t_{i,calc}$ the measured and calculated thicknesses in point y_i and $z_{i,meas}$ and $z_{i,calc}$ the corresponding z-values. The relative maximal errors are calculated as the absolute maximal error divided by the mean value:

$$e_{t,max,\%} = \frac{e_{t,max}}{\bar{t}_{meas}} * 100 \text{ and } e_{z,max,\%} = \frac{e_{z,max}}{\bar{z}_{meas}} * 100. \quad (5)$$

The same equations hold for the relative mean errors in Tables 2 and 3.

Table 2 shows the results for the comparison of the measured and calculated thickness distributions. The errors in this table are calculated at constant y-values (vertical direction in Figure 4). The mean absolute thickness error for all experiments is 0.0182 mm, which corresponds to a relative error of 1.47% of the mean thickness measured by the fringe projection scanner. The largest errors from the measured thickness distributions occur in areas with high wall angles and at high curvatures, i.e., at the boundary between the walls and the bottom of the workpiece in the concave (and straight) shapes and the boundary at the clamping in the convex shapes. Errors in these areas can go up to a maximum of 0.1688 mm (in the vertical direction for the convex pyramid on Figure 4(f)). The corresponding relative errors in the y-direction go up to 13.69 % of the mean measured thickness. In case of the convex cone, these high errors are reached due to a measurement peak close to the clamping. In case of the concave cone and pyramid, the large errors are due to a small horizontal shift of the peak, resulting in higher vertical errors at high wall angles.

Table 2: Errors for the calculated *thickness distributions* compared to the measured ones at constant y-values.

Name	Max absolute error [mm] $e_{t,max}$	Relative max error [%] $e_{t,max,\%}$	Mean absolute error [mm] $e_{t,mean}$	Relative mean error [%] $e_{t,mean,\%}$	Standard deviation [mm] std $(\overrightarrow{e_t})$
Concave cone	0.0951	7.87 %	0.0289	2.39 %	0.0197
Concave pyramid	0.0843	6.86 %	0.0134	1.09 %	0.0199
Straight cone	0.0846	6.61 %	0.0204	1.60 %	0.0169
Straight pyramid	0.0403	3.24 %	0.0074	0.59 %	0.0078
Convex cone	0.1266	10.32 %	0.0231	1.89 %	0.0202
Convex pyramid	0.1688	13.69 %	0.0159	1.29 %	0.0219
Average	0.0999	8.10 %	0.0182	1.47 %	0.0177

Table 3 and the section geometry comparisons in Figure 4 show that the geometric errors of the section measured with DIC and with fringe projection are not large and do not have significant influence on the errors between the calculated and measured thickness distributions. These geometric errors of the z-coordinates (calculated at constant y-values) can go up to 1.5064 mm difference, which corresponds to 4.34 % of the mean measured z-value.

Table 3: Errors for the *geometries* measured with DIC and with fringe projection compared at constant y-values.

Name	Max absolute error [mm] $e_{z,max}$	Relative max error [%] $e_{z,max,\%}$	Mean absolute error [mm] $e_{z,mean}$	Relative mean error [%] $e_{z,mean,\%}$	Standard deviation [mm] std $(\overrightarrow{e_z})$
Concave cone	1.0493	3.58 %	0.6019	2.05 %	0.2574
Concave pyramid	1.2800	4.15 %	0.9317	3.02 %	0.1398
Straight cone	1.5064	4.34 %	1.3040	3.76 %	0.2071
Straight pyramid	1.1775	3.33 %	0.8914	2.52 %	0.1447
Convex cone	1.0402	2.58 %	0.7477	1.86 %	0.1033
Convex pyramid	1.3106	3.25 %	0.9874	2.45 %	0.1207
Average	1.2273	3.54 %	0.9107	2.61 %	0.1622

Table 4 shows the minimal thicknesses measured by the fringe projection scanner and calculated from the DIC measurements. The minimal thickness occurs in the most critical areas, and is a valid indicator for part failure. The values in this table are calculated using the following formulas:

$$\bar{t}_{meas} = \frac{\sum_{i=1}^{N} t_{i,meas}}{N},\ \bar{t}_{calc} = \frac{\sum_{i=1}^{N} t_{i,calc}}{N},\ t_{min,meas} = \min(\vec{t}_{meas}), \tag{6}$$

$$t_{min,calc} = \min(\vec{t}_{calc}),\ e_{t,min} = t_{min,meas} - t_{min,calc} \text{ and } e_{t,min,\%} = \frac{e_{t,min}}{t_{min,meas}} * 100. \tag{7}$$

The errors of the calculated minimal thicknesses for all experiments are on average -2.87% of the mean measured thickness, which corresponds to a thickness overestimation of 0.0206 mm. For all shapes except for the straight cone and pyramid, this minimal thickness is estimated higher than its real measured value. The measuring peak in the convex pyramid (Figure 4(f)) results in the highest relative underestimation of 11.10% of the mean measured thickness and is caused by the close distance to the backing plate.

Table 4: Mean and min thicknesses from DIC and fringe projection and the errors on the minimal thickness calculations.

Name	Mean thickness measured [mm] $\bar{t}_{meas}$	Mean thickness calculated [mm] $\bar{t}_{calc}$	Min thickness measured [mm] $t_{min,meas}$	Min thickness calculated [mm] $t_{min,calc}$	Min error [mm] $e_{t,min}$	Relative min error [%] $e_{t,min,\%}$
Concave cone	1.2072	1.2272	0.8279	0.8415	-0.0136	-1.65 %
Concave pyramid	1.2287	1.2337	0.8530	0.8837	-0.0308	-3.61 %
Straight cone	1.2794	1.2684	1.2367	1.1930	0.0437	3.53 %
Straight pyramid	1.2457	1.2432	1.2111	1.2081	0.0030	0.25 %
Convex cone	1.2263	1.2098	0.8335	0.8720	-0.0385	-4.62 %
Convex pyramid	1.2331	1.2434	0.7874	0.8748	-0.0874	-11.10 %
Average	1.2368	1.2376	0.9583	0.9789	-0.0206	-2.87 %

No significant differences in thickness calculations and measurements can be detected between the conical and pyramidical shapes, even though in the conical shapes a higher strain in the second principal direction (ϵ_2) is present due to an additional curvature in the tangential direction. The results in Figure 4 show no significant differences, except for the convex parts close to the boundary where the part is clamped (Figure 4(e) and (f) at y=80-90 mm). These differences are mostly due to a different clamping, with the conical shapes clamped further from the part with a diameter of 197 mm instead of the squared clamping shape of 184 mm in the pyramids. The measurements with the fringe projection scanner can be affected a bit by the backing plate in case of the pyramids.

Conclusion

The thickness distributions calculated from the DIC surface strains align well with the measured thickness distributions, with a mean error of 0.0182 mm (a mean percentage of 1.47 % of the mean measured thickness distributions). Maximal thickness errors go up to 0.1688 mm (measured at constant y-value), which corresponds to a maximum relative thickness error of 13.69 % of the mean measured thickness. Hence, the DIC strains can be used to estimate the thickness distributions, but care must be taken in regions of high wall angles and curvatures. Characterizing the thickness of a part based on DIC measurements leads to functionally useful results. The minimal calculated thicknesses have an average relative error of -2.87 % of the measured minimal thickness, which corresponds to an overestimation of the minimal calculated thickness.

Acknowledgements

Marthe Vanhulst was supported by a Predoctoral Strategic Basic Research Fellowship of the Research Foundation—Flanders (FWO) with project 1S47622N.

References

[1] J. Jeswiet, F. Micari, G. Hirt, A. Bramley, J. Duflou, and J. Allwood, "Asymmetric Single Point Incremental Forming of Sheet Metal," *CIRP Ann. - Manuf. Technol.*, 2005, doi: 10.1016/S0007-8506(07)60021-3.

[2] J. Verbert *et al.*, "Multi-Step toolpath approach to overcome forming limitations in single point incremental forming," *Int. J. Mater. Form.*, vol. 1, no. S1, pp. 1203–1206, Apr. 2008, doi: 10.1007/s12289-008-0157-2.

[3] J. Gu, H. Sol, S. He, A. Van Bael, and J. Duflou, "Full field optical measurement of large deformation fields in Single Point Incremental Forming (SPIF) Processes," *Abstr. ATEM Int. Conf. Adv. Technol. Exp. Mech. Asian Conf. Exp. Mech.*, vol. 2007.6, no. 0, p. _OS9-1-1-1-_OS9-1-1-6, 2007, doi: 10.1299/jsmeatem.2007.6._os9-1-1-1.

[4] I. Vasilakos, J. Gu, B. Belkassem, H. Sol, J. Verbert, and J. R. Duflou, "Investigation of deformation phenomena in spif using an in- process DIC technique," in *Key Engineering Materials*, 2009, vol. 410–411, pp. 401–409, doi: 10.4028/www.scientific.net/KEM.410-411.401.

[5] K. Jawale, J. F. Duarte, A. Reis, and M. B. Silva, "Characterizing fracture forming limit and shear fracture forming limit for sheet metals," *J. Mater. Process. Technol.*, vol. 255, pp. 886–897, May 2018, doi: 10.1016/j.jmatprotec.2018.01.035.

[6] P. Shrivastava and P. Tandon, "Enhancement of fracture forming limit by crystallographic texture reformation of AA1050 sheets in Single Point Incremental Forming," in *IOP Conference Series: Materials Science and Engineering*, Nov. 2019, vol. 651, no. 1, p. 012074, doi: 10.1088/1757-899X/651/1/012074.

[7] V. K. Barnwal, S. Chakrabarty, A. Tewari, K. Narasimhan, and S. K. Mishra, "Forming behavior and microstructural evolution during single point incremental forming process of AA-6061 aluminum alloy sheet," *Int. J. Adv. Manuf. Technol.*, vol. 95, no. 1–4, pp. 921–935, Mar. 2018, doi: 10.1007/s00170-017-1238-5.

[8] N. Decultot, L. Robert, V. Velay, and G. Bernhart, "Single point incremental sheet forming investigated by in-process 3D digital image correlation," *EPJ Web Conf.*, vol. 6, p. 11001, Jun. 2010, doi: 10.1051/epjconf/20100611001.

[9] P. Eyckens *et al.*, "Strain evolution in the single point incremental forming process: Digital image correlation measurement and finite element prediction," *Int. J. Mater. Form.*, vol. 4, no. 1, pp. 55–71, Mar. 2011, doi: 10.1007/s12289-010-0995-6.

[10] B. Van Mieghem, P. Lava, D. Debruyne, A. Van Bael, and J. Ivens, "Digital image correlation for on-line wall thickness measurements in thick gauge thermoforming," in *Key Engineering Materials*, 2013, vol. 554–557, pp. 1583–1591, doi: 10.4028/www.scientific.net/KEM.554-557.1583.

[11] B. Van Mieghem, J. Ivens, and A. Van Bael, "Consistency of Strain Fields and Thickness Distributions in Thermoforming Experiments Through Stereo DIC," *Exp. Tech. 2016 405*, vol. 40, no. 5, pp. 1409–1420, Aug. 2016, doi: 10.1007/S40799-016-0143-4.

[12] M. M. Gonzalez, N. A. Lutes, J. D. Fischer, M. R. Woodside, D. A. Bristow, and R. G. Landers, "Analysis of geometric accuracy and thickness reduction in multistage incremental sheet forming using digital image correlation," in *Procedia Manufacturing*, 2019, vol. 34, pp. 950–960, doi: 10.1016/j.promfg.2019.06.105.

[13] J. Verbert, "Computer Aided Process Planning for Rapid Prototyping With Incremental Sheet Forming Techniques (Computer ondersteunde proces planning voor rapid prototyping met incrementele plaatvormtechnieken)," Katholieke Universiteit Leuven, 2010.